

# The stability of a zonally averaged thermohaline circulation model

G.A. Schmidt and L.A. Mysak

Centre for Climate and Global Change Research  
and  
Department of Atmospheric and Oceanic Sciences  
McGill University  
805 Sherbrooke St. W, Montreal, QC, H3A 2K6, Canada

Revised for Tellus  
Mar 1995

## ABSTRACT

A combination of analytical and numerical techniques are used to efficiently determine the qualitative and quantitative behaviour of a one-basin zonally averaged thermohaline circulation ocean model under various forcing regimes and over a large region of parameter space. In contrast to earlier studies which use time stepping to find the steady solutions, the steady state equations are first solved directly to obtain the multiple equilibria under identical mixed boundary conditions. This approach is based on the differentiability of the governing equations and especially the convection scheme. A linear stability analysis is then performed, in which the normal modes and corresponding eigenvalues are found for the various equilibrium states. Resonant periodic solutions superimposed on these states are predicted for various types of forcing.

The results are used to gain insight into the solutions obtained by Mysak, Stocker and Huang in a previous numerical study in which the eddy diffusivities were varied in a randomly forced one-basin zonally averaged model. It is shown that the two-cell symmetric circulation is generally unstable to anti-symmetric perturbations in the temperature or salinity (as expected), and that both one-cell (inter-hemispheric) circulation patterns are generally stable. Resonant stable oscillations with century scale periods are predicted with structures that compare favorably with those found in the previous study. In cases with large horizontal diffusivities, the two-cell pattern is also stable, which parallels cases in the previous study where large vacillations were seen between the three stable steady states. Further, in cases with large horizontal *and* large vertical diffusivities, no one-cell pattern can be realised and the only asymptotic behaviour found is the two-cell pattern.

An experiment is also performed to examine the effect of varying the restoring time constants in the relaxation boundary conditions used at the surface for both salinity and temperature.

## 1. Introduction

Multiple equilibria of the thermohaline ocean circulation (THC) under mixed boundary conditions (restoring condition for temperature, a flux condition for salinity) have been found in many recent theoretical studies. In examples ranging from simple Stommel-type box models (Stommel, 1961; Cessi, 1994) to full general circulation models (GCMs) (Manabe and Stouffer, 1988; Weaver and Sarachik, 1991), various steady states of the circulation can exist under identical forcing. In the box models, both temperature and salinity dominant states are found, with one circulation being the reverse of the other. In full GCMs, depending on the geometry used, both northern sinking and southern sinking states are among those seen (see Weaver and Hughes (1992) for a review).

A question that arises is how relevant are these models (and the various THC states) for the actual thermohaline circulation? Also, how robust are the multiple equilibria, and how much do they depend upon the various simplifications and parameterisations used in the models? If the models are relevant, then the question of the stability of the equilibria becomes crucial.

The past approach to answering these questions has either been analytic (from a non-linear dynamics standpoint) or purely numeric. The analytic approach can provide a complete description of the behaviour in only the relatively simple models (see for instance Maas (1994)). The numeric approach (Bryan, 1986) provides much less complete information, but it can deal with much more complex cases. One barrier to providing a more complete determination of the behaviour of the complex models is the exhausting (computational) effort needed to explore the full model parameter space which is frequently 6- or 7-dimensional. Another factor to be considered is the sensitivity of the solutions to the initial conditions.

This paper demonstrates a *methodology* that can be used to analyse the stability of the more complicated numerical models by invoking analytical techniques more normally applied to systems with many fewer degrees of freedom. Many models can be accurately characterised by the number and nature of the steady states of the model. Hence by using a methodology which concentrates on these states, it is hoped that the effect of parameter changes and different initial conditions can be more clearly seen.

To illustrate the advantages of this methodology, the stability of the Wright and Stocker (1991) zonally averaged THC model is investigated. This model has been successfully employed in various ocean climate (Stocker and Wright, 1991; Wright and Stocker, 1992) and paleoclimatic (Stocker *et al.*, 1992) studies. When under random forcing (Mysak *et al.*, 1993) (hereafter MSH), the one-basin model exhibits century scale fluctuations superimposed on a basic one-cell circulation pattern (with either northern sinking or southern sinking). For large horizontal eddy diffusivities a two-cell symmetric circulation can persist.

In contrast to the numerical approach used in the past in which the model is

time stepped to equilibrium, here the various steady solutions are found *directly*. The steady state equations are first solved under restoring conditions and a salinity flux diagnosed as before. Then the steady equations are solved under the new flux condition for salinity. The methodology which is fully explained in §2 centrally depends on the differentiability of the governing equations and specifically the convection scheme. It should be added that since this is a highly non-linear problem, there is always some uncertainty as to whether all the steady states have been found. Isolated steady states often exist which cannot be found simply by tracing the path of the known steady states through the parameter space. In this case there is possibly another steady state that has a collapsed thermohaline circulation (i.e., one with no deep water formation). However, this is difficult to stimulate and hence there is doubt as to whether it exists in the one-basin model used here (though it has been seen in a two-basin model (Stocker and Wright, 1991)).

Once a steady state has been found, a linear stability analysis is performed. This will determine whether the steady state found is stable or not, and if not, what are the fastest growing modes. Also, information is obtained about the nature of possible oscillations (growing, neutrally stable or damped) and the frequencies associated with them. These modes and the associated frequencies provide all the information needed to describe the small amplitude behaviour of the model under various forcing regimes around a given steady state. For a particular forcing frequency, the complete solution for the resultant periodic solution can be written down. Certain frequencies will cause a resonant response, and it is those frequencies that will be most evident under stochastic (white-noise) forcing. In this way, a qualitative picture can be built up of the behaviour of the model which is hopefully more robust than the quantitative results gained from simply running the model to equilibrium in different parameter regimes and from various initial states.

As various parameters change, the stability criteria will also change; the points in parameter space at which these changes occur (bifurcations) are also where new forms of asymptotic behaviour can emerge. For instance, there can be a change from stability to instability (through a pitchfork bifurcation) implying new steady states. Similarly, a change from damped to growing oscillations (through a Hopf bifurcation) implies the existence of a finite limit cycle, although the analysis of the resulting periodic solutions requires more sophisticated tools than will be presented here.

If this analysis can be used to explain the behaviour in an already investigated problem, then it can be used to *predict* the behaviour in different parameter regimes or with different boundary conditions without the need to run the model for thousands of computer years.

As a first test, the methodology is applied to the work of MSH mentioned above. In that paper a small-amplitude stochastic forcing was added to the freshwater flux in each surface grid cell, and the eddy diffusivities were varied over a wide range. In a large region of parameter space, oscillations with century-scale periods were seen to be induced around various steady states. The results in §3 indicate that these oscillations

can be accurately represented by resonant modes of a linearised model centred on the steady states. MSH also showed that very long (millennial) period vacillations could be induced between steady states (including the two-cell circulation). The results here indicate that these vacillations are only induced at points at which the intermediate two-cell circulation is stable and where there are three competing basins of attraction.

A second set of experiments are presented in which the restoring times used in the temperature and salinity boundary conditions were varied. In the past, investigators have followed Haney (1971) who used heat and energy flux arguments to derive a relaxation boundary condition for temperature which used a time constant of around 50 days. His argument amounted to assuming that the atmosphere had an infinite heat capacity (i.e., the surface air temperature does not change). It has been pointed out by Schopf (1983) and by Zhang *et al* (1993) that in comparison with the ocean, the atmosphere has a very small heat capacity and that therefore a zero heat capacity atmosphere might be more suitable. Such a model also implies that a restoring boundary condition for temperature should be used but with a much longer restoring time, around 600 days. Use of this formulation has been shown to prevent the collapse of the thermohaline circulation upon the switch to mixed boundary conditions in GCMs (the so-called polar halocline catastrophe) (Zhang *et al*, 1993). This collapse is similar to the what happens to the initial two-cell circulation in the one-basin zonally averaged model, but with the crucial difference that the two-cell pattern is not close to the observed state of the present THC.

In the spin up of ocean models (including GCMs) a restoring condition is also used for the salinity. This has no physical basis and should be seen merely as data assimilation in order to deduce a salinity flux (evaporation/precipitation) at some steady state similar to today's ocean. The restoring time used for this is usually the same as for the temperature. However, Tziperman *et al* (1994) have recently argued that such a short restoring time constrains the salinity field too highly. They argue that given the accuracy to which the surface salinity concentration is known, a restoring time of at least 120 days should be used. As above, the collapse of the thermohaline circulation in GCMs upon a change to mixed boundary conditions, can be avoided with such a restoring time.

The stability of the solutions for various values for both restoring time constants are examined using a similar procedure as followed in Experiment 1. As was found for the GCMs, a longer restoring time for temperature does lead to a more stable state, but the qualitative features of the solutions remain unaffected.

This paper is structured as follows. In §2 an outline is given of how a local linearisation of the model can be used to solve the steady state equations and how the behaviour of the model near a steady state can be approximated. The results from the first experiment, where the eddy diffusivities are varied over a large range (following MSH), are contained in §3.

Section 4 describes the results from the second set of experiments (varying the restoring time constants). In §5 a general discussion of the methodology used and its

utility for further studies is given. In an appendix some of the more technical aspects of the new convection scheme used are derived and discussed.

## 2. The model and experimental procedure

The model used in this study is a variant of that developed by Wright and Stocker (1991) (hereafter WS). This is a zonally averaged model and since the ocean basin has boundaries, there remains a term in the equations related to the east-west pressure gradient. To close the problem, WS assume that this can be written as a function of the north-south pressure gradient with constant of proportionality  $\epsilon$ , the pressure gradient closure parameter (see p1716 in WS for further details). The most significant difference in the model used here is that a new convection scheme is used. The original WS model (in common with many GCMs (Marotzke, 1991)) uses a highly non-linear scheme at each time step which mixes boxes depending on the static stability at each interface. This process can take a number of passes through a column to obtain a statically stable state. There are a number of disadvantages to this process in terms of finding steady states and determining the linear stability. For example, the mixing is an analogue for the amount of convection that would take place in a given time step; hence if an attempt is to be made to determine steady states *without time stepping the model*, i.e. with  $\Delta t = 0$ , then this procedure is not helpful. The step-function-like behaviour at every point in this scheme (full convection or no convection) means that it is very non-linear and non-differentiable. As a consequence, it is impossible to determine analytically the effect of a small perturbation in the temperature or salinity fields on the convective flux. A more suitable parameterisation would be one in which the convective heat and salt transports were independent of the time step used and differentiable with respect to density in each box. One such scheme (derived and discussed in Appendix A) has been used throughout this paper. This uses a vertical diffusion coefficient ( $K_v$ ) which varies smoothly from a small value (indicating eddy diffusion) to a large spatially-varying one (representing convection) as the density gradient at the interface between two boxes changes. The scheme is differentiable at every point with respect to the densities above and below the interface.

The convection scheme used here leads to slightly altered flows as compared to those in WS; however, the conclusions of previous work still hold. All the other parameters, i.e. the surface restoring time, the surface boundary conditions, the closure parameter and the resolution, are identical to those considered previously.

As mentioned in the introduction, the steady states of the model are found directly rather than by time-stepping the equations. This is a procedure commonly followed in studies of dynamical systems and is straightforward once the spatial parts of the equations have been discretised (using the method outlined in Fiadiero and Veronis (1977) and extended by Wright (1992)). The original infinite-dimensional partial differential system is approximated by an  $N$ -dimensional system, where  $N = 2mn$  and  $m, n$  are the number of vertical and horizontal grid boxes respectively. In each

box the potential temperature ( $T$ ) and salinity ( $S$ ) are free variables. The other variables in the problem  $\rho$  (density) and  $\Psi$  (streamfunction) are dependent on  $T$  and  $S$ .

A variant of the standard procedure (Bryan, 1969) for running an ocean model is used. The steady state equations with restoring boundary conditions on temperature and salinity are first solved using Newton's method and a salinity flux is then deduced. This flux is then used as the surface condition for salinity and the equations are solved again with these mixed boundary conditions. Judicious variation of the initial guess can be used to find different steady solutions under those mixed conditions.

It is helpful to arrange the independent variables as a vector  $\mathbf{x} = (S_{11}, S_{12}, \dots, S_{21}, \dots, S_{mn}, T_{11}, \dots, T_{mn})$ . Then the advection-diffusion equations for both temperature and salinity can be written concisely as

$$\dot{\mathbf{x}} = F(\Psi, K_h, K_v)\mathbf{x},$$

or using summation convention

$$\dot{x}_i = F_{ij}(\Psi, K_h, K_v)x_j, \quad i = 1, N \quad (1)$$

where  $F$  is a matrix, whose coefficients depend on  $\Psi, K_h$  and  $K_v$ , and represents the fluxes due to advection, horizontal and vertical eddy diffusion, convection and the boundary conditions. The vertical diffusion coefficient,  $K_v$ , is to be understood as including the effects of convection as outlined in the Appendix. The non-linearities arise through the dependence of  $\Psi$  and  $K_v$  on  $\mathbf{x}$  by way of the density. Fortunately  $F$  is sparse and therefore relatively easy to deal with.

For small disturbances,  $\delta\mathbf{x}$ , around any state  $\mathbf{x}$ , (1) can be expanded in a Taylor series,

$$\dot{x}_i + \delta\dot{x}_i = F_{ij}x_j + F_{ij}\delta x_j + \left\{ \frac{\partial F_{ij}}{\partial \Psi_k} \delta \Psi_k + \frac{\partial F_{ij}}{\partial K_v} \delta K_v \right\} x_j + O(|\delta\mathbf{x}|^2), \quad i = 1, N \quad (2)$$

and since  $\Psi$  and  $K_v$  are functions of  $\mathbf{x}$ , (2) can be written as

$$\dot{x}_i + \delta\dot{x}_i = F_{ij}x_j + F_{ij}\delta x_j + \left\{ \frac{\partial F_{ij}}{\partial \Psi_k} \frac{\partial \Psi_k}{\partial x_l} + \frac{\partial F_{ij}}{\partial K_v} \frac{\partial K_v}{\partial x_l} \right\} \delta x_l x_j + O(|\delta\mathbf{x}|^2). \quad i = 1, N \quad (3)$$

The validity of this approach depends crucially upon the fact that model equations (and specifically the convection scheme) are differentiable. Collecting together the perturbation quantities, (3) can be simplified to

$$\dot{x}_i + \delta\dot{x}_i = F_{ij}x_j + A_{ij}\delta x_j + O(|\delta\mathbf{x}|^2), \quad i = 1, N. \quad (4)$$

where  $A_{ij} = F_{ij} + (\partial F_{il} / \partial \Psi_k)(\partial \Psi_k / \partial x_j)x_l + (\partial F_{il} / \partial K_v)(\partial K_v / \partial x_j)x_l$ . With the mixed boundary conditions, there is a slight complication since there is the extra condition

that the total salinity content of the ocean remains constant. This implies that the matrix  $A$  as defined above is singular, (i.e., one equation in (4) is a linear combination of the others). This just reduces the number of independent variables by one, so the equations are rewritten by eliminating one of the perturbation salinity variables. All the following equations then hold.

Equation (4) can be used in two ways. If  $\mathbf{x}$  is near a steady state and a closer approximation is needed, then setting the LHS of (4) to zero and solving for  $\delta\mathbf{x}$  gives

$$\delta x_i = -(A^{-1})_{ij} F_{jk} x_k, \quad (5)$$

which generally gives a better estimate to the steady state. This is simply Newton's method for finding roots. Alternatively, if  $\mathbf{x}$  is a steady state then

$$\dot{x}_i = F_{ij} x_j = 0, \quad (6)$$

and (4) can be solved to determine the stability and fastest growing perturbations (given by the eigenvalues ( $\lambda_i$ ) and eigenvectors ( $\mathbf{x}_i$ ) of  $A$ ) of the steady state. It should be noted that the steady state found under restoring conditions remains a steady state upon a switch to the derived flux condition (i.e. the matrix  $F$  does not change). However the matrix  $A$  does change and hence so do the stability characteristics. All linear stability analyses are done under mixed boundary conditions.

Newton's method is the most effective method to use to find a zero of a non-linear multi-dimensional system of equations if the differentials can be found analytically (Press *et al*, 1990). It converges quadratically to the root provided the initial guess is good enough, but it does have rather poor global convergence and so some insight into what kind of solution is expected helps, (this can be gained from a time-stepping model). Most importantly, it will converge to a steady state *regardless* of whether that state is stable or unstable, unlike a time-stepped model. On occasion, Newton's method fails to converge, settling instead on a repeating cycle around the steady state. Usually this can be alleviated by using an initial guess closer to the desired solution.

Whenever a steady state has to be found numerically it is important to get as close as possible to the real steady state before performing a linear stability analysis. The eigenvalues found will correspond more accurately to those at the steady state the closer one is to that point. A linear stability analysis away from a steady point gives information about how neighbouring trajectories behave (i.e., how the phase space volume is locally evolving) and can give misleading information about the stability of the (nearby) steady state. For instance, near a two dimensional saddle point there may be points where (locally) the phase space volume is reducing in time and hence a linear stability analysis there would misleadingly indicate stability.

With knowledge of  $A$  and hence the linear stability criteria, we effectively have a linear model at a tangent to the full model, valid near a steady state. Hence, if forcing is added to (1) and if it has a small enough amplitude, the linear equations (4) will describe the ensuing motion as long as the perturbation remains small.



Specifically, if the forcing used is similar to white-noise (all frequencies present), the linearisation allows us to examine the contribution of each frequency separately. Furthermore, since the equations decouple if written in terms of the normal modes (the eigenvectors of  $A$ ), the resonance response of each normal mode for each forcing frequency can be found. Take the case of a normal mode  $\mathbf{x}_i$  with a corresponding complex eigenvalue  $\lambda_i + i\omega_i$ . Given forcing at a particular frequency  $\omega$ , the equation governing the evolution of the complex amplitude ( $y_i$ ) of that mode is

$$\dot{y}_i - (\lambda_i + i\omega_i)y_i = F_i e^{i\omega t}. \quad (7)$$

The (possibly complex)  $F_i$  is the component of the forcing projected onto this normal mode. If the normal mode is damped then the long term behaviour of  $y_i$  will be governed by the (periodic) particular solution of this equation. This solution has a maximum amplitude (given unit forcing at all frequencies) when  $\omega = \sqrt{(\omega_i^2 - \lambda_i^2)}$ , the resonant frequency. If  $|\lambda_i| > |\omega_i|$  then the mode is critically damped and the largest amplitude response occurs at  $\omega = 0$ . However, if the normal mode is *sub-critical* with  $|\lambda_i| < |\omega_i|$  the largest amplitude response occurs at the resonant frequency. Hence, if white-noise forcing is used the periodic solution at the resonant frequency would be the largest significant response. These periodic solutions are stable if and only if the steady state around which they oscillate is also stable (i.e.  $\lambda_i < 0$  for all  $i$ ). This gives an estimate of the dominant periods of oscillation around a steady state. It could be that there are no sub-critical modes in which case the linear response will resemble red noise (high frequencies damped) with no significant peaks.

Once the linear stability has been established efforts are made to determine where in parameter space there are changes to the stability. These are points at which a stable steady state becomes unstable, such as when the horizontal diffusivity decreases. At these points, there are bifurcations to different asymptotic forms of behaviour. There can be branching of solutions leading to different (stable or unstable) steady states or from a stable state to a limit cycle (a Hopf bifurcation). This will be discussed further in §5.

### 3. Experiment 1: Variation of the eddy diffusivities

MSH used the WS model with low-amplitude stochastic forcing at the surface to find the flows corresponding to a number of different values for the eddy diffusivities. They found century-scale periodic oscillations around various steady states for typical values of the diffusivities and large vacillations between steady states when the horizontal diffusivity was relatively large. This first experiment repeats the runs performed in MSH but with the revised convection scheme and the new methodology described in the previous section.

### 3.1 Specification

The range of values taken for the vertical and horizontal eddy diffusivities ( $K_{v-eddy}$ ,  $K_h$ ) is the same as in MSH. Henceforth the vertical eddy diffusivity is written as  $K_v$  to correspond to previous work, but it should not be confused with the non-constant  $K_v$  mentioned in the previous section and Appendix. The steady state equations for the model are first solved using restoring boundary conditions on temperature and salinity with a time constant of 70 days. The salinity and temperature profiles used in the restoring conditions are the same as used previously and are an approximation to the present day climatological averages for the Atlantic. This forces a two-cell symmetric circulation pattern. From this solution a salinity flux is derived which is then applied as the surface boundary condition for the salinity.

Next, the steady state equations are solved with the new boundary condition and, by choosing a suitable initial guess, a one-cell northern sinking circulation pattern is found. For completeness, the models were also led to converge to a southern sinking pattern. However, since the models were symmetric this was the exact reverse of the northern sinking pattern. As would be expected the method converged to the two-cell pattern (even if unstable) if the initial guess was close or the one-cell pattern did not exist. The linear stability of the steady states was determined using the procedure outlined in the previous section.

The resolution, pressure gradient closure parameter  $\epsilon$  and time step were all fixed at 15 horizontal boxes and 9 vertical levels, 0.5 and 14 days respectively as in MSH. The basin stretched from 80°N to 80°S, the horizontal eddy diffusivity  $K_h$  was one of 1,2,5,10 or 15 ( $\times 10^3$ )  $\text{m}^2\text{s}^{-1}$  while the vertical eddy diffusivity  $K_v$  was chosen from among 1,2,4 and 10 ( $\times 0.5 \times 10^{-4}$ )  $\text{m}^2\text{s}^{-1}$ .

### 3.2 Results

To discuss the results, it will be convenient to refer to each of the cases by an ordered pair referring to the vertical and horizontal diffusivities. Thus the ordered pair (4,5) refers to the case where  $K_v = 4 \times 0.5 \times 10^{-4} \text{ m}^2\text{s}^{-1}$  and  $K_h = 5 \times 10^3 \text{ m}^2\text{s}^{-1}$ . The canonical diffusivity case mentioned in MSH corresponds to the pair (2,1). Under restoring conditions, the results (outlined in Table 1) show that in all cases the method converged to a symmetric two-cell circulation pattern (see Fig. 1) from which the salinity flux at the surface could be determined.

The results of the linear stability calculation in which the perturbation field is  $\propto \exp(\lambda t)$  (Table 2) show that except for large  $K_h$  the two-cell pattern under mixed boundary conditions is unstable. Complex eigenvalues imply the existence of slowly growing or damped oscillatory components. As the horizontal diffusivity increases, the magnitude of the largest positive eigenvalue decreases and passes through the origin for  $K_h$  between 5 and  $10 \times 10^3 \text{ m}^2\text{s}^{-1}$  and then stays negative. For these larger values of  $K_h$  the two-cell circulation is *stable*. This is confirmed by time-stepping the

model with the salinity flux condition in the high  $K_h$  cases and seeing that the model stays with a two-cell pattern. This implies that there is a curve in the diffusivity parameter space across which there is a change of stability and hence a bifurcation to other steady states. If a close approximation to the critical parameter values can be found then the bifurcation point could be examined and the nature of the branching steady states determined.

The eigenvector for a given diffusivity pair corresponding to the eigenvalue with largest positive real part is the fastest growing perturbation. Any initial perturbation to the steady state can be expressed as a linear combination of all the eigenvectors, but with time the coefficients of the other eigenvectors will grow more slowly or decay and only the most unstable eigenvector will remain (provided the amplitude is sufficiently small so that the regime is still linear). These unstable eigenvectors for the two-cell circulation for the different diffusivity pairs are all very similar and are anti-symmetric in the temperature and salinity fields. This corresponds to a strengthening of one of the cells over the other (depending on the sign of the mode coefficient). An example of the salinity perturbation for the unstable mode in the case (2,1) is given in Fig. 2. The temperature field has much the same structure although it is the salinity field that dominates the density perturbation. The streamfunction anomaly is single-signed and thus corresponds to an increase in the circulation of one cell over the other, (which one depends on the initial perturbation). Since the two-cell circulation gives a symmetric distribution for salinity and temperature (see Fig. 1) this instability is symmetry breaking.

The oscillatory eigenvectors represent modes which all have symmetric temperature/salinity/density perturbations, as seen for example in Fig. 3. Periods range between 400 and 700 years and  $e$ -folding time scales between 400 to 1000 years. The eigenvectors are complex ( $\mathbf{v}_r \pm i\mathbf{v}_i$ ) and the perturbations over a period follow the pattern  $\mathbf{v}_r \rightarrow -\mathbf{v}_i \rightarrow -\mathbf{v}_r \rightarrow \mathbf{v}_i \rightarrow \mathbf{v}_r$  etc. (Note that the picture on the RHS of Fig. 3 is the imaginary part of the eigenfunction and therefore corresponds to the perturbation after a quarter period multiplied by -1). The associated streamfunction perturbations are antisymmetric and thus correspond to simultaneous increases (or decreases) in the overturning of the two cells.

In all the cases where the two cell circulation is unstable there are normal modes that are sub-critical. If the system is forced, these modes would resonate at century-scale periods, but since there are unstable modes (some eigenvalues with positive real part), these resonant forced periodic solutions are unstable to small disturbances and would not be realised in practice. There were no sub-critical modes found in the cases where the two-cell circulation was stable. As the damping increases (the real part of the eigenvalue becomes more negative), the structure of the eigenvectors increases in complexity.

With the new mixed boundary conditions the steady state equations were solved using a suitable initial condition to coax it to a northern sinking pattern. In most of the cases the model converged successfully to such a one-cell pattern, all of which

were similar to the equilibrium for the case (2,1) shown in Fig. 4. There is a tendency for a minor southern sinking cell (e.g. in case (10,10) with a maximum overturning streamfunction of about 1/5 that of the larger cell) to appear at the surface as the diffusivities become larger. The maximum value of the streamfunction found in each case is given in Table 3, which can be compared with Table 1 in MSH. In two cases, (4,15) and (10,15), the solution always converged to the two-cell pattern and we conjecture that there is no one-cell steady state in these cases, (had the state merely been unstable, Newton's method should have converged to it).

The flow associated with the slowest decaying mode (the smallest negative eigenvalue) for the one-cell pattern represents a slowing down or speeding up of the one-cell circulation without, however, changing the structure. As noted previously, higher modes have more complex structures.

Cases that are of particular interest here are those that have sub-critical normal modes. In many cases corresponding to smaller values of the horizontal diffusivity, there exist just one pair of sub-critical modes (Table 5). The periods at which they resonate (included in the table) correspond very well with the dominant frequencies seen in MSH. In MSH, the dominant period for the (2,1) canonical diffusivity case was 227 yrs which is close to the 286 yrs predicted here. Similarly, the (1,1) case has a period of 250 yrs in MSH, which again is just under the 285 yrs here. This implies that the oscillations around steady states seen in MSH are very close to being linear.

An example from case (4,1) of the sub-critical oscillatory perturbation is shown in Figs. 5 and 6. What is the mechanism for this oscillation? The flow of the basic state is very similar to that shown in Fig. 4 so the advection of anomalies by the main flow is northward at the surface and southward at depth. If we examine the surface negative salinity anomaly in Fig. 5a, it is clear that a quarter of a period later it has been subducted into the down-welling zone (Fig. 5b) and that a further quarter of a period later it is entirely submerged (Fig. 5c). It takes approximately 3 (900 yrs) periods to go completely around, which is a reasonable overturning time for a one-basin ocean. As the anomaly is advected its magnitude decreases after it is down-welled and increases only after it reaches the surface again. In the absence of forcing, the initial perturbation has an  $e$ -folding time of only 50 years (about a quarter of a period) so this oscillation is not self sustaining. With forcing at the surface of the right frequency the weak salinity anomalies at the surface in the South can be amplified as they are advected northward.

Figure 5 should be compared with Fig. 10 in MSH where salinity anomalies in the (2,1) case are similarly advected north, down-welled and diffused in the deep ocean.

The linear perturbations seen here are made up of two separate effects; the advection by the basic flow of the perturbation temperature and salinity fields and secondly, the advection by the perturbation streamfunction field of the basic temperature and salinity fields. The anomaly in the streamfunction corresponding to the salinity anomaly in Fig. 5a is shown in Fig. 6. The perturbation is mostly confined to the deep ocean where the basic state of the temperature and salinity is roughly

constant. Hence the advection of the basic field by the anomalous streamfunction plays only a minor rôle in the oscillation.

What does all this tell us about the likely behaviour of the model under low-amplitude random forcing? If this forcing is assumed to be temporally and spatially uncorrelated, all modes will be excited more or less equally. The existence of the purely real or critically damped complex modes implies that the largest response of these modes will occur when the forcing frequency tends to zero. Hence the spectrum of the output of the model will be skewed towards red-noise. However, in the case where sub-critical oscillatory modes exist, the largest response is at the non-zero resonant frequency and so a peak at this frequency above the red noise would be expected. The structure of the oscillation will then be very close to that of the sub-critical normal mode. Variation from this pattern would be expected if the random forcing increased in amplitude so that the linearisation was no longer valid. Even if the forcing was low-amplitude, the resonance response could have a large amplitude and non-linearities would again become important. In this case, there is some scope for a weakly non-linear analysis which would allow amplitude dependence based on a harmonic balance type approach (see for instance Chapters 5 and 7 of Jordan and Smith (1977)). This topic will be treated in a future paper.

Interestingly enough, the analysis also shows that for large  $K_h$  the two-cell pattern becomes more stable and that for some cases, e.g. (1,15) and (2,15), there are three stable steady states. Comparing this situation to the large vacillations seen for the (1,15) case in MSH indicates that in the latter paper the two-cell pattern seems to be an attractor. It is tempting to suggest that in cases where the two-cell pattern is unstable, low-amplitude random forcing is unlikely to provoke a switch between the two one-cell patterns, but where it is *stable*, switches between them via the two-cell pattern are more likely, (cf Fig. 5 and Fig. 6 in MSH). Determining the periods of these highly non-linear vacillations is obviously beyond the scope of a linear analysis.

### 3.3 Summary

It is helpful to quickly summarise and compare the results predicted here with those seen in MSH. However, it must be borne in mind that the samples of results given in MSH are not complete and that there are subtle but real differences in the coding of the two models.

The experimental procedure in MSH precluded any stable two-cell circulations being seen immediately after the switch to the mixed boundary conditions, (large salinity anomalies were added to the northernmost cell to encourage convection there). There is, however, some indirect evidence from the forced solutions that the two-cell circulation was stable in at least the cases (1,15) and (10,15). This is also seen in this study.

Only in the case of (10,15) was there no evidence in MSH of a more than marginally stable one-cell circulation. Here, for this case, no one-cell circulation could be found.

Where significant century-scale periods were seen in MSH in the spectra for cases (1,1) and (2,1), namely 250 and 227 yrs, we find sub-critical modes with periods of 285 yrs and 286 yrs respectively. Overall both studies see a decrease in century scale periodic behaviour as both  $K_h$  and  $K_v$  increase. Generally, the amplitudes of the response of the model used in MSH increases linearly with the amplitude of the random forcing. This indicates that the linearised approach taken here is valid.

In the only long time integration performed by MSH (in the (1,15) case), three stable steady states were clearly seen, precisely as predicted here.

Differences between the two studies are also worth noting. In some cases (e.g. (4,1), (4,2) and (10,1)) we predict that century scale oscillations should occur around the one-cell circulation, although there does not seem to be such a peak in the spectra for these cases in MSH. Also, there is clearly a stable one-cell circulation in the case (4,15) in MSH but we were unable to find it here. Further, we predict that the two-cell steady state is stable in both the 10 and  $15 \times 10^3 \text{m}^2 \text{s}^{-1} K_h$  cases but as stated above, evidence for this is only shown for the two cases (1,15) and (10,15).

Possible reasons for these differences are discussed in §5.

## 4. Experiment 2: Variation of the restoring time constants

The standard boundary condition for temperature used in ocean models states that the heat flux at the surface,  $Q$ , is proportional to the difference between the ocean surface temperature,  $T$ , and the apparent atmospheric temperature,  $T_a$ . The constant of proportionality can be written as  $\Delta z / \tau_T$ , where  $\Delta z$  is the depth of the first grid point and  $\tau_T$  is a restoring time constant for the temperature. Depending on the derivation of this boundary condition (assuming an infinite or zero heat capacity atmosphere) the  $\tau_T$  can have values ranging from 50 to 600 days. The apparent atmospheric temperature takes into account the effects of evaporation and solar radiation but is close to the actual equilibrium atmospheric temperature almost everywhere except at the equator (Haney, 1971). Since we are only using an analytic approximation to the atmospheric temperature, the distinction need not concern us. The restoring boundary condition for salinity is generally written in the same manner.

The experiment carried out below is a simple test of the sensitivity of the zonally averaged thermohaline circulation model to changes in the values of the restoring time constants  $\tau_T$  and  $\tau_S$ . The values chosen ranged from 50 days to 600 days and the same procedure as in experiment 1 was followed. Strictly speaking, the apparent atmospheric variables have different interpretations depending on the derivation used, but for this simple experiment it will suffice to use the same form for each.

### 4.1 Specification

In this experiment the effect of different restoring times for the salinity and temperature  $\tau_S, \tau_T$  on the one-basin circulation is studied. The values of 50, 300 and 600

days are used for each (see Table 6) and the same apparent atmospheric temperature or salinity profiles are used throughout.

The eddy diffusivities and closure parameter used are taken from Wright and Stocker (1992);  $K_h = 1 \times 10^3 \text{m}^2 \text{s}^{-1}$ ,  $K_v = 0.5 \times 10^{-4} \text{m}^2 \text{s}^{-1}$  and  $\epsilon = 0.45$ , while the other factors and procedures remain as in experiment 1.

#### 4.2 Results

Under restoring boundary conditions, the solution in all cases converged on the two-cell pattern, as occurred in §3, and the salinity flux was then diagnosed. Generally, the shorter the restoring time, the more constrained the field. Therefore, since the temperature and salinity fields are diffusive, a longer restoring time implies a reduction in the surface gradients of the field. The THC is driven by the equator-to-pole temperature gradients but opposed by the salinity gradients, so we would expect a decrease in the value of the overturning streamfunction as  $\tau_T$  increased and an increase as  $\tau_S$  increases. This is precisely what is seen in Table 6 although the variations are relatively slight. The maximum absolute value of the streamfunction for the two-cell circulation is not very sensitive to the two parameters. The structure of the steady state in all cases is very similar to the example shown in Fig. 1.

A linear stability analysis (Table 7) of the two-cell circulation does reveal some significant differences between the cases, particularly when the surface temperature is relatively highly constrained. There is clearly an increase in stability as the value of  $\tau_T$  increases (in good agreement with the results of Zhang *et al*, 1993). However, in contrast with the conclusions of Tziperman *et al* (1994), there is no general increase in stability with  $\tau_S$ . For  $\tau_T$  of 50 days (Table 7) and for the cases  $\tau_T$  of 30 days and  $\tau_S$  of 30 or 120 days (not shown), the results show a *decrease* in the stability with  $\tau_S$ . This is reversed for larger values of  $\tau_T$  and if the constants are increased together there is a consistent increase in stability. However, the two-cell circulation never (for these parameter values) becomes absolutely stable upon a switch to mixed boundary conditions.

The remarkable increase in the growth rates for the  $\tau_T = 50$  days case as  $\tau_S$  increases deserves further comment. A further analysis of this case done with many more values of  $\tau_S$  indicated that there is a smooth increase with  $\tau_S$  of the growth rate. However, the structure of the most unstable normal mode is strikingly different at the two extremes. Generally, the most unstable mode has an anti-symmetric structure in the salinity and temperature fields (cf Fig. 2) and the perturbation is seen over the whole domain. In contrast, the most unstable modes in the  $\tau_S = 600$  day case are very localised in the polar regions. The streamfunction perturbations associated with these represent intense and localised high latitude up/down-welling. The reason for this lies in the minor differences that occur in the density structure as  $\tau_S$  increases. Since the salinity gradients reduce with  $\tau_S$ , boxes in the polar regions have a higher salinity and this serves to actually reverse the surface density gradient there. The densest

surface boxes now occur one grid box away from the boundary and most convection and downward advection occurs there (Fig. 7). The top few polar boxes on the other hand are now isolated from the main flow and become neutrally stable. Note that the convection scheme (as described in the appendix) has the highest gradient with density at this point. Hence, the linear stability analysis upon a switch to mixed boundary conditions shows that any positive density anomaly causes (proportionately) a very large increase in  $K_v$ , the diffusion coefficient. Indeed, further tests on these cases show that there is a high sensitivity of the growth rate with the convection parameters. This effect is then mainly an artifact of the convection scheme used but one that does not occur in more standard cases.

The salinity fluxes derived for the different restoring times vary only slightly. They decrease in magnitude by a few percent (mainly at the equator) with both increasing  $\tau_S$  and  $\tau_T$ . As a consequence the maximum value for the streamfunction in the final one-cell circulation under mixed conditions is almost completely insensitive to the restoring time used for the salinity boundary condition (Table 8). The slight decrease in the circulation as the temperature restoring time constant increases can be explained by a weakening of the N-S density gradient caused by a weaker temperature gradient which occurs because the surface water does not react as quickly to the atmosphere. There is also little variation in the largest eigenvalues for the one-cell steady state as  $\tau_S$  increases (Table 9). However, there is a small decrease in the stability as  $\tau_T$  increases. This is to be expected since the dominant perturbations from the steady state will tend to persist longer as the restoring time increases.

As would be expected in light of Table 5, there are sub-critical modes for these cases that would be expected to resonate given suitable forcing. The results in Table 10 show that, surprisingly, there does seem to be a large dependence on the value of  $\tau_S$  used in the spin up. This indicates that these higher modes are more sensitive to the structure and magnitude of the derived salinity flux. As before, the increase in period with  $\tau_T$  is due to a weakening of the restoring force on any perturbation.

In conclusion, it seems that this zonally-averaged model has only a mild sensitivity on the restoring times used. The stabilising tendencies noted by previous investigators of increased  $\tau_T, \tau_S$  seem to be borne out (except for the one anomalous case due to the highly delicate nature of the convection scheme). In contrast to the GCM results, in no case does the solution arrived at under restoring boundary conditions actually become stable.

## 5. Conclusions

A new methodology has been used in this paper to examine the behaviour of a one-basin zonally-averaged thermohaline circulation model. The model is based on the equations and parameterisations introduced by Wright and Stocker (1991), but modified to include a smooth (differentiable) convection scheme. Instead of time-stepping the model to equilibrium as in earlier studies, the steady state equations are



first solved directly using Newton’s method under both restoring and mixed boundary conditions. This has the advantage of greatly increased efficiency and achieves much better accuracy in solving the spatially discretised equations. A much more detailed picture of how the model behaves in various parameter regions can be built up in a fraction of the time needed when using the spin-up approach. A linear perturbation analysis of the steady states then gives information about the absolute stability of the states, the nature and structure of the fastest growing modes and what kind of oscillatory solutions might be expected. Specifically, the period and structure of any resonance response is readily found. The existence of the multiple states does not depend upon the preliminary run under restoring conditions before a salinity flux has been deduced. In fact, if a suitable salinity flux is prescribed independently, an unstable two-cell steady state can still be found.

In §3, it was shown that this methodology has the ability to efficiently reproduce and explain results that were previously (and laboriously) calculated by time stepping the Wright and Stocker model under low-amplitude stochastic surface forcing (Mysak *et al.*, 1993). There is a high degree of correspondence between the results of MSH and those presented here with regard to determining the absolute stability of each state, the characteristics of each state and the resonant century scale oscillations. The minor differences are most probably explained by a slight decrease in the (numerical) diffusivity of the present model because of the different convection scheme. The conclusion drawn is that (in this model at least) the thermohaline circulation can resonate with century-scale periods around various steady states and that these oscillations are characterised by the amplification of surface salinity anomalies and their advection around the basin.

A comparison of the conclusions made here concerning the bifurcations of this model can be made with other two-dimensional (non-rotating) THC models studied by other investigators, specifically Thual and McWilliams (1992) and Quon and Ghil (1992). For large values of the diffusion coefficients, the model presented here has only one steady state, a stable two-cell circulation pattern. A cross-section through the bifurcation surface is shown in Fig. 8. The ratio between the horizontal and vertical diffusivities is kept fixed at  $3 \times 10^7$  and the vertical diffusivity is increased slowly from  $0.5 \times 10^{-3} \text{m}^2 \text{s}^{-1}$  to  $7.5 \times 10^{-3} \text{m}^2 \text{s}^{-1}$ . For small values of the coefficients there exist two stable one-cell patterns and an unstable two-cell pattern. As the coefficients increase the two-cell circulation pattern becomes stable, and as they increase further the one-cell circulation patterns disappear. It is likely that there is a pitchfork bifurcation as the stability of the two-cell pattern changes which connects the paths; however no evidence was found for these intermediate unstable steady states. In the Thual and McWilliams model there is a very similar bifurcation pattern seen (Figure 3 in their paper) but with an additional salinity-dominated steady state not present here. A symmetric temperature dominant steady state becomes unstable at some critical parameter and bifurcates to a two mutually opposite one-cell circulations which only exist for a limited parameter range. A similar pattern is also seen in the Quon and Ghil

model. As the thermal Raleigh number (inversely proportional to the temperature diffusion coefficient) increases, a symmetric two-cell circulation bifurcates *smoothly* to an increasingly asymmetric one-cell dominant pattern (see their Figures 14 and 16). Hence, it seems that the bifurcation structure seen in two-dimensional THC models is quite robust.

The work in experiment 2 dealing with different restoring times for the temperature and salinity relaxation boundary conditions indicates that the circulation changes very little as the time constants change over an order of magnitude. One possible explanation for the disparity between this result and that of Tziperman *et al* (1994) is that changes in the restoring times will likely have an effect on three dimensional processes with shorter time scales (i.e., over a few years) which are not represented in the Wright and Stocker model. Hence any changes of stability found in GCMs as  $\tau_T$  and  $\tau_S$  vary, are unlikely to be found in this model. This implies the rather welcome conclusion that the eventual steady states or long term behaviour of the 2-D model is not crucially dependent on the spin up process or on the exact formulation of the relaxation boundary conditions. In one case with a large  $\tau_S$  but small  $\tau_T$ , there was an anomalously large growth rate for perturbations to the two-cell circulation. This was due to a small pool of near-neutrally stable water collecting at the poles which could be triggered to start convecting with only a small salinity perturbation. This subsequent large linear growth rate is hence very sensitive to the details of the convection scheme. Note that for large growth rates the time for which the linear approximation is valid will be much smaller than in other cases.

Other limitations of this work should also be mentioned. Most interesting behaviour is non-linear (large amplitude), and if a linear analysis is to provide any kind of qualitative indications of asymptotic behaviour it must be complete, i.e. *all* the steady states should be found and an attempt made to describe the phase paths. However, there is no certain way of knowing whether that point has been reached. Also, if higher amplitude forcing is used, then the linear modes are only useful as a first approximation to the non-linear resonance response and give no information about the much more rich behaviour of even a weakly non-linear model. There is some scope for analytical results in the weakly non-linear regime and this will be discussed in a future paper. Notwithstanding these caveats, the methodology presented here has proved to be an efficient way of describing the behaviour of a 2-D model. It would be interesting in future work to examine the stability of the solutions when there are two or more basins connected by an Antarctic Circumpolar Current. In particular, are the century scale oscillations still prevalent? The effect of relative basin widths could also be clearly examined. It could also be worthwhile to try and apply the same methodology to three dimensional models.

## 6. Acknowledgments

This work was supported by research grants awarded to LAM from NSERC and

Fonds FCAR. The authors are grateful for the helpful comments received from two anonymous referees.

## Appendix A: Derivation of a differentiable convection scheme

As an alternative to the explicit mixing algorithm used by Wright and Stocker (1991), an attempt is made to determine the convective flux produced by their scheme and translate it into an equivalent diffusive flux which would vary smoothly with the densities of the grid boxes. The basic idea can be made clear by considering a column of two overlying boxes with fluid of different densities.

Assume that the fluid at the interface is unstably stratified, hence a convective correction must be made. According to the explicit mixing scheme, the potential temperature and salinity of the two boxes will be averaged and each box will now have identical characteristics. For each box let  $\Delta z_i, T_i$  and  $S_i$  be the (fixed) depth of the box, the box-averaged potential temperature and the box-averaged salinity respectively, where  $i = 1, 2$ . The new  $T$  and  $S$  for the boxes can then be written as

$$T = \frac{\Delta z_1 T_1 + \Delta z_2 T_2}{\Delta z_1 + \Delta z_2}, \quad S = \frac{\Delta z_1 S_1 + \Delta z_2 S_2}{\Delta z_1 + \Delta z_2}.$$

This implies heat and salt transports between the boxes *over one time step* of

$$M_T = \frac{\Delta z_1 \Delta z_2 (T_2 - T_1)}{\Delta z_1 + \Delta z_2},$$

and

$$M_S = \frac{\Delta z_1 \Delta z_2 (S_2 - S_1)}{\Delta z_1 + \Delta z_2}.$$

If there were solely a diffusive flux, using a second order flux-conservative finite difference scheme (specifically the scheme outlined by Fiadiero and Veronis (1977) and generalised by Wright (1992)) would imply vertical fluxes of

$$F_T = \frac{2K(T_2 - T_1)}{\Delta z_1 + \Delta z_2},$$

and

$$F_S = \frac{2K(S_2 - S_1)}{\Delta z_1 + \Delta z_2},$$

through the interface.

The effective diffusion coefficient of the convective scheme is then determined by equating the two expressions for the fluxes after taking account of the time step, i.e.

$$K_{conv} = \frac{\Delta z_1 \Delta z_2}{2\Delta t}, \tag{A.1}$$

This is the diffusion that would have been required to operate over the time step specified to give the same effect as the explicit convection scheme.

It is also possible to find similar expressions in the case where there are three boxes in a column. For this situation the effective diffusion coefficients at the two boundaries between the cells are

$$K_{conv}^1 = \frac{\Delta z_1 \Delta z_2}{2\Delta t} \frac{(\Delta z_1 + \Delta z_2)}{(\Delta z_1 + \Delta z_2 + \Delta z_3)}, \quad (A.2a)$$

$$K_{conv}^2 = \frac{\Delta z_2 \Delta z_3}{2\Delta t} \frac{(\Delta z_2 + \Delta z_3)}{(\Delta z_1 + \Delta z_2 + \Delta z_3)}, \quad (A.2b)$$

for boxes 1 and 2 and boxes 2 and 3 respectively.

For more than three boxes, there is no equivalence of convection and diffusion since the explicit convection scheme takes into account all the values of the temperature and salinity over the column. Such non-local effects cannot be modelled using only a second order scheme. However the form of the effective diffusion in the two and three box cases suggests that a diffusion coefficient proportional to the depth of two neighbouring boxes and inversely proportional to the time step might produce similar results. For example, at the boundary between the  $i$ th and  $i+1$ th boxes, the diffusion coefficient could take the form

$$K_{conv}^i = \lambda \frac{\Delta z_i \Delta z_{i+1}}{\Delta t}. \quad (A.3)$$

In the two box case  $\lambda = 1/2$ , and in the three box case  $\lambda \approx 1/3$  (depending on the relative sizes of the boxes). The key point is to choose a value for lambda that gives the most consistent results. There are some restrictions on the value of  $\lambda$  since numerical instability will result if the diffusion is too large. There is also a lower limit on the effective diffusion since it must be greater than the eddy diffusion coefficient being used, probably by an order of magnitude. If  $\lambda$  is taken to be 0.5 in the full model then the numerical scheme is unstable. Various experiments with different values lead to the conclusion that the maximum  $\lambda$  consistent with stability over a range of time steps and grid spacings is  $\lambda = 1/3$ . The results from using this scheme and the explicit scheme in the model are qualitatively and quantitatively similar and hence it is used exclusively in the examples in the text.

The vertical diffusion coefficient used at any interface now depends in a consistent way on the static stability criteria (the sign of  $\rho_z$ ) at that interface. There is still a discontinuity at the point where  $\rho_z = 0$  which has to be smoothed out if a fully differentiable scheme is required. Physically this can be justified by considering the unresolved variations in density on both sides of the interface. It is entirely probable that the conditions for convection will occur at points on the interface without the average cell densities being statically unstable. Hence the flux of heat and salt will increase over that generated solely by eddy diffusion ( $K_{v-eddy}$ ) as neutral stability is approached. Therefore, we have chosen to use a tanh-like functional form for the vertical diffusion i.e.

$$K_v^i = K_{v-eddy} \exp \left( \frac{1}{2} \log \left( \frac{K_{conv}^i}{K_{v-eddy}} \right) (\tanh(\gamma(\rho_i - \rho_{i+1})) + 1) \right) \quad (A.4)$$

where the parameter  $\gamma$  determines how steep the smoothing is. This form for the vertical diffusion has the properties that it tends to  $K_{v-eddy}$  for very stable conditions and to  $K_{conv}$  as static instability occurs. Exponential functions are included since the values of  $K_{v-eddy}$  and  $K_{conv}$  can differ by orders of magnitude and with a simple linear smoothing  $K_v$  increases much too rapidly. The results using this form are robust as long as  $\gamma$  is sufficiently large (greater than about  $30/\rho_0 \text{ m}^3\text{kg}^{-1}$ ). A uniform value of  $50/\rho_0 \text{ m}^3\text{kg}^{-1}$  is used throughout this paper.

There seems to be a contradiction in using this scheme to solve the steady state equations because of the explicit dependence on the time-step  $\Delta t$  in (A.3). However, this has the effect of ensuring that the *flux* associated with the convection does not depend on  $\Delta t$  and that this flux only depends on the density differences. There is a plausible argument that says that this time constant should be associated with the time scales of actual convective events. Experiments with various reasonable  $\Delta t$  values show very little difference in the steady states found as  $\Delta t$  varied from 1 day to 2 months ( $\Delta t$  in time-stepped model runs is usually about 14 days).

## References

- Bryan, F. 1986. High latitude salinity effects and interhemispheric thermohaline circulation. *Nature*, **323**, 301–304.
- Bryan, K. 1969. A numerical method for the study of the circulation of the world ocean. *J. Comput. Phys.*, **4**, 347–376.
- Cessi, P. 1994. A simple box model of stochastically forced thermohaline flow. *J. Phys. Oceanogr.*, **24**, 1911–1920.
- Fiadiero, M. E. and Veronis, G. 1977. On weighted-mean schemes for the finite-difference approximation to the advection-diffusion equation. *Tellus*, **29**, 512–522.
- Haney, R. L. 1971. Surface thermal boundary condition for ocean circulation models. *J. Phys. Oceanogr.*, **1**, 241–248.
- Jordan, D. W. and Smith, P. 1977. *Non-linear Ordinary Differential Equations*. Oxford Applied Mathematics and Computing Science Series. Oxford University Press.
- Maas, L. R. M. 1994. A simple model for the three-dimensional, thermally and wind driven ocean circulation. *Tellus*, **46A**, 671–680.
- Manabe, S. and Stouffer, R. J. 1988. Two stable equilibria of a coupled ocean atmosphere model. *J. Climate*, **1**, 841–866.
- Marotzke, J. 1991. Influence of convective adjustment on the stability of the thermohaline circulation. *J. Phys. Oceanogr.*, **21**, 903–907.

- Mysak, L. A., Stocker, T. F., and Huang, F. 1993. Century-scale variability in a randomly forced, two-dimensional thermohaline ocean circulation model. *Climate Dynamics*, **8**, 103–116.
- Press, W. H., Flannery, B. P., Teukolsky, S. A., and Vetterling, W. T. 1990. *Numerical Recipes*. Cambridge University Press.
- Quon, C. and Ghil, M. 1992. Multiple equilibria in thermosolutal convection due to salt-flux boundary conditions. *J. Fluid Mech.*, **245**, 449–483.
- Schopf, P. S. 1983. On equatorial waves and El Niño. II: Effects of air-sea thermal coupling. *J. Phys. Oceanogr.*, **13**, 1878–1893.
- Stocker, T. F. and Wright, D. G. 1991. A zonally averaged ocean model for the thermohaline circulation. Part II: Inter-ocean circulation in the Pacific-Atlantic basin system. *J. Phys. Oceanogr.*, **21**, 1725–1739.
- Stocker, T. F., Wright, D. G., and Mysak, L. A. 1992. A zonally averaged coupled ocean-atmosphere model for paleoclimatic studies. *J. Climate.*, **5**, 773–797.
- Stommel, H. 1961. Thermohaline convection with two stable regimes of flow. *Tellus*, **13**, 224–230.
- Thual, O. and McWilliams, J. C. 1992. The catastrophe structure of thermohaline convection in a two-dimensional fluid model and a comparison with low-order box models. *Geophys. Astrophys. Fluid Dynamics*, **64**, 67–95.
- Tziperman, E., Toggweiler, J. R., Feliks, Y., and Bryan, K. 1994. Instability of the thermohaline circulation with respect to mixed boundary conditions: Is it really a problem for realistic models? *J. Phys. Oceanogr.*, **24**, 217–232.
- Weaver, A. J. and Hughes, T. 1992. Stability and variability of the thermohaline circulation and its link to climate. *Trends in Phys. Oceanogr., Council of Scientific Research Integration, Trivandrum, India*.
- Weaver, A. J. and Sarachik, E. S. 1991. The role of mixed boundary conditions in numerical models of the ocean’s climate. *J. Phys. Oceanogr.*, **21**, 1470–1493.
- Wright, D. G. 1992. Finite difference approximations to the advection-diffusion equation. *Tellus*, **44A**, 261–269.
- Wright, D. G. and Stocker, T. F. 1991. A zonally averaged ocean model for the thermohaline circulation. Part I: Model development and flow dynamics. *J. Phys. Oceanogr.*, **21**, 1713–1724.
- Wright, D. G. and Stocker, T. F. 1992. Sensitivities of a zonally averaged global ocean circulation model. *J. Geophys. Res.*, **97**, 12707–12730.
- Zhang, S., Greatbatch, R. J., and Lin, C. A. 1993. A re-examination of the Polar Halocline Catastrophe and implications for coupled ocean-atmosphere modelling. *J. Phys. Oceanogr.*, **23**, 287–299.

**Table 1:** The maximum absolute value for the stream function (in Sv) at steady state for each pair of diffusivities under restoring boundary conditions. This corresponds to a two-cell circulation pattern.

$K_v$ Vertical diffusivity ( $\times 0.5 \times 10^{-4} \text{ m}^2\text{s}^{-1}$ )	$K_h$ Horizontal diffusivity ( $\times 10^3 \text{ m}^2\text{s}^{-1}$ )				
	1	2	5	10	15
1	5.95	5.59	4.97	4.41	3.94
2	9.03	9.14	8.35	7.17	6.48
4	14.2	13.9	13.3	11.8	10.5
10	25.3	25.2	24.5	22.7	20.5

**Table 2:** The values of the two largest eigenvalues (in  $(100 \text{ year})^{-1}$ ) in the linear stability analysis of the two-cell circulation pattern under mixed boundary conditions. Positive (negative) values indicate an unstable (stable) state and complex values indicate growing or damped oscillations. As both  $K_v$  and  $K_h$  increase, the two-cell state becomes more stable.

$K_v$ Vertical diffusivity ( $\times 0.5 \times 10^{-4} \text{ m}^2\text{s}^{-1}$ )	$K_h$ Horizontal diffusivity ( $\times 10^3 \text{ m}^2\text{s}^{-1}$ )				
	1	2	5	10	15
1	2.20	1.87	1.09	-0.02	-0.30
	$0.75 \pm i0.87$	$0.39 \pm i1.24$	$-0.73 \pm i1.71$	-0.34	-0.95
2	1.77	1.62	0.95	-0.09	-0.46
	$0.27 \pm i1.47$	$0.07 \pm i1.68$	-0.44	-0.46	-1.07
4	1.24	1.03	0.50	-0.38	-0.38
	-0.38	-0.40	-0.41	-0.41	-1.28
10	0.66	0.53	0.13	-0.68	-0.69
	-0.56	-0.57	-0.51	-0.69	-1.55

**Table 3:** The maximum absolute value for the stream function (in Sv) at steady state for each pair of diffusivities under the mixed boundary conditions (cf. Table 1 in MSH). These results are for a one-cell northern-sinking circulation pattern. No values are given for the (4,15) or (10,15) cases because these always converged to the two-cell pattern as described in the text.

$K_v$ Vertical diffusivity ( $\times 0.5 \times 10^{-4} \text{ m}^2\text{s}^{-1}$ )	$K_h$ Horizontal diffusivity ( $\times 10^3 \text{ m}^2\text{s}^{-1}$ )				
	1	2	5	10	15
1	11.6	11.1	9.8	8.2	6.3
2	18.0	17.4	15.8	13.5	10.5
4	26.7	26.1	24.3	21.3	-
10	45.0	44.0	40.9	35.3	-

**Table 4:** The value of the two largest eigenvalues (in  $(100 \text{ year})^{-1}$ ) in the linear stability analysis of the one-cell circulation pattern. All values have negative real parts hence all the states examined are stable but complex values indicate (damped) oscillations. No values are given for the (4,15), (10,15) cases since no estimate of the one-cell circulation could be found.

$K_v$ Vertical diffusivity ( $0.5 \times 10^{-4} \text{ m}^2\text{s}^{-1}$ )	$K_h$ Horizontal diffusivity ( $10^3 \text{ m}^2\text{s}^{-1}$ )				
	1	2	5	10	15
1	-0.09	-0.10	-0.11	-0.09	-0.17
	$-0.38 \pm i0.20$	$-0.45 \pm i0.17$	-0.44	-0.36	-0.70
2	-0.15	-0.16	-0.17	-0.17	-0.18
	$-0.53 \pm i0.32$	$-0.62 \pm i0.32$	$-0.86 \pm i0.25$	-0.70	-0.62
4	-0.24	-0.24	-0.24	-0.27	-
	$-0.70 \pm i0.49$	$-0.78 \pm i0.49$	-0.94	$-1.32 \pm i0.47$	-
10	-0.48	-0.47	-0.44	-0.43	-
	$-1.35 \pm i0.58$	$-1.22 \pm i0.60$	$-1.48 \pm i0.79$	$-1.49 \pm i0.68$	-



**Table 5:** For the one-cell circulation, some cases associated with smaller eddy diffusivities have normal modes that are *sub-critical*, i.e., they are not critically damped and hence have resonant frequencies. These frequencies are those that would be expected to dominate the response of the system under white-noise forcing. The century-scale periods for cases (1,1) and (2,1) compare favorably with those seen in the model runs of MSH.

Frequencies of sub-critical modes and their resonant periods					
$K_v$ Vertical diffusivity ( $0.5 \times 10^{-4} \text{ m}^2\text{s}^{-1}$ )	$K_h$ Horizontal diffusivity ( $10^3 \text{ m}^2\text{s}^{-1}$ )				
	1	2	5	10	15
1	$-1.12 \pm i2.47$ 285 yrs	$-1.21 \pm i2.14$ 353 yrs	-	-	$-6.49 \pm i7.10$ 218 yrs
2	$-1.75 \pm i2.80$ 286 yrs	$-1.77 \pm i2.49$ 359 yrs	-	-	-
4	$-2.34 \pm i3.16$ 296 yrs	$-2.42 \pm i2.84$ 423 yrs	-	-	-
10	$-3.41 \pm i3.61$ 526 yrs	-	-	-	-

**Table 6:** The maximum absolute value for the stream function (in Sv) at steady state for each pair of restoring time values under restoring conditions. This corresponds to a two-cell circulation pattern. There is a slight tendency for the circulation to increase with  $\tau_S$  and to decrease with  $\tau_T$  but both the pattern and magnitude of the circulation are relatively stable.

$\tau_T$ Temperature restoring time (days)	$\tau_S$ Salinity restoring time (days)		
	50	300	600
50	5.71	5.98	6.45
300	5.68	5.84	6.03
600	5.57	5.71	5.87

**Table 7:** The value of the two largest eigenvalues (in  $(100 \text{ year})^{-1}$ ) in the linear stability analysis of the two-cell circulation pattern. Positive values indicate an unstable state and complex values indicate (growing or damped) oscillations.

$\tau_T$ Temperature restoring time (days)	$\tau_S$ Salinity restoring time (days)		
	50	300	600
50	2.17 $0.78 \pm i0.76$	18.9 16.8	44.4 44.4
300	0.84 -0.11	0.65 -0.11	0.44 -0.11
600	0.44 -0.07	0.28 -0.07	0.13 -0.07

**Table 8:** The maximum absolute value for the stream function (in Sv) at the steady state under the mixed boundary conditions. This corresponds to a one-cell circulation pattern. There is a slight tendency for the circulation to decrease with  $\tau_T$  and  $\tau_S$  but as for the two-cell circulation the pattern and magnitude of the circulation seem relatively stable.

$\tau_T$ Temperature restoring time (days)	$\tau_S$ Salinity restoring time (days)		
	50	300	600
50	11.2	11.1	10.9
300	10.8	10.8	10.7
600	10.4	10.3	10.3

**Table 9:** The value of the largest eigenvalues (in  $((100 \text{ year})^{-1})$ ) in the linear stability analysis of the one-cell circulation pattern. There is almost no variation with the  $\tau_S$  used in the spin up; however, as  $\tau_T$  increases the one-cell state becomes slightly less stable due to the reduction in the surface restoring force.

$\tau_T$ Temperature restoring time (days)	$\tau_S$ Salinity restoring time (days)		
	50	300	600
50	-0.10	-0.10	-0.10
300	-0.06	-0.06	-0.06
600	-0.05	-0.05	-0.05

**Table 10:** The period (in years) associated with the sub-critical normal mode at resonance. In contrast to table 9, there is a relatively large variation in the resonant periods with  $\tau_S$ . This indicates a higher degree of sensitivity to the salinity flux boundary condition. The increase of period with  $\tau_T$  is to be expected due to the reduction in the strength of the restoring condition.

$\tau_T$ Temperature restoring time (days)	$\tau_S$ Salinity restoring time (days)		
	50	300	600
50	300	320	390
300	520	700	-
600	1900	-	-

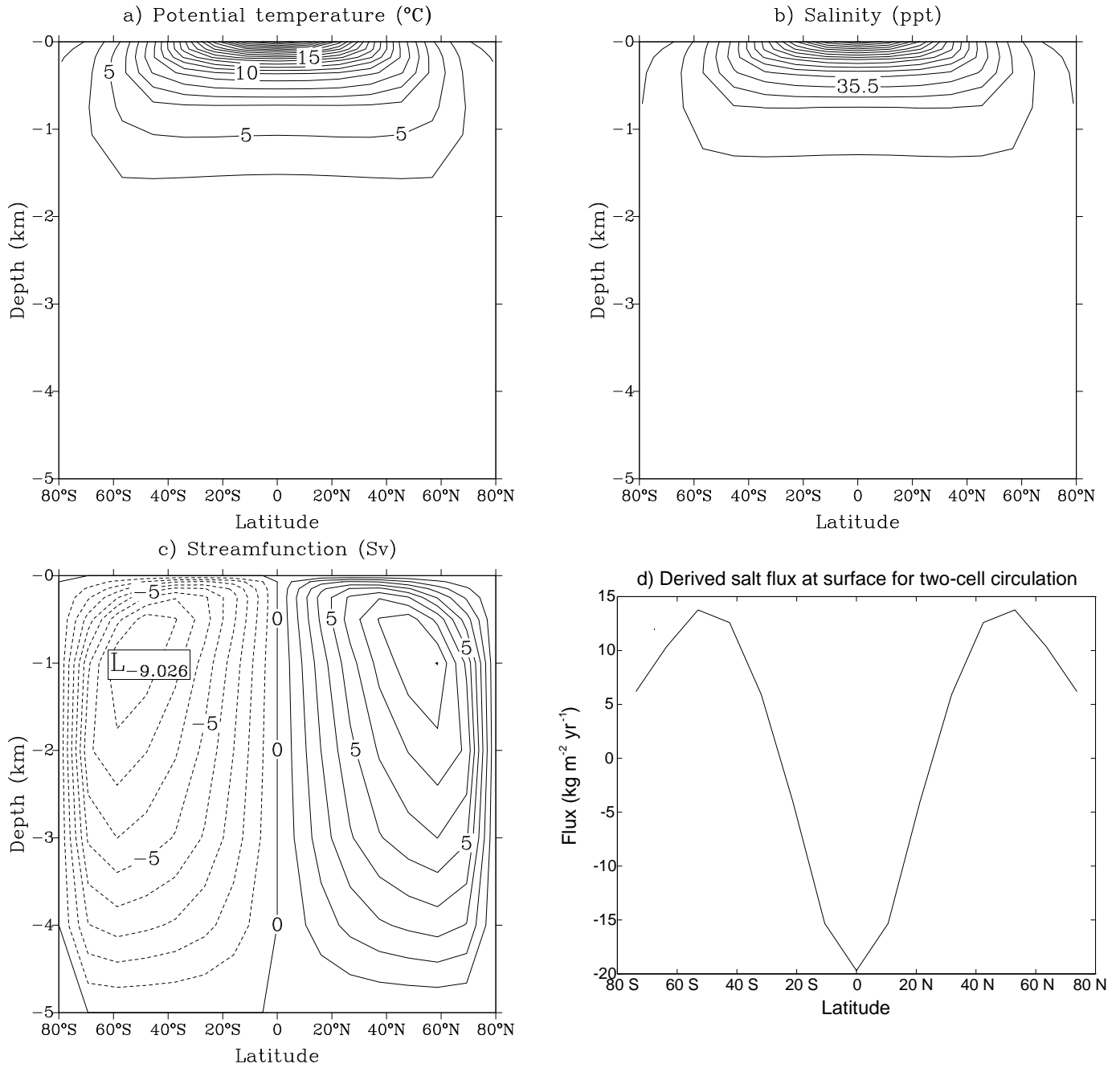


**Figure 1:** The (a) Temperature, (b) salinity (contour interval 0.1 ppt), (c) streamfunction and (d) derived salinity flux for the two cell circulation in the (2,1) (the so-called canonical diffusivities) case. This symmetric circulation is reached after solving the equations under restoring boundary conditions.

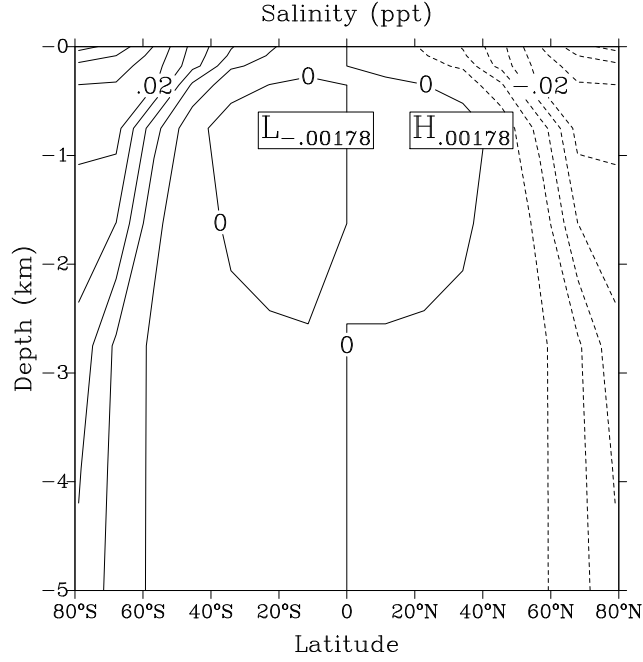


**Figure 2:** The salinity perturbation that corresponds to the fastest growing (non-oscillatory) mode for the two-cell circulation in the (2,1) (canonical diffusivities) case. This mode is anti-symmetric and thus causes one cell to become larger than the other which finally leads to the one-cell circulation seen in Fig. 4. The corresponding temperature perturbation is very similar.

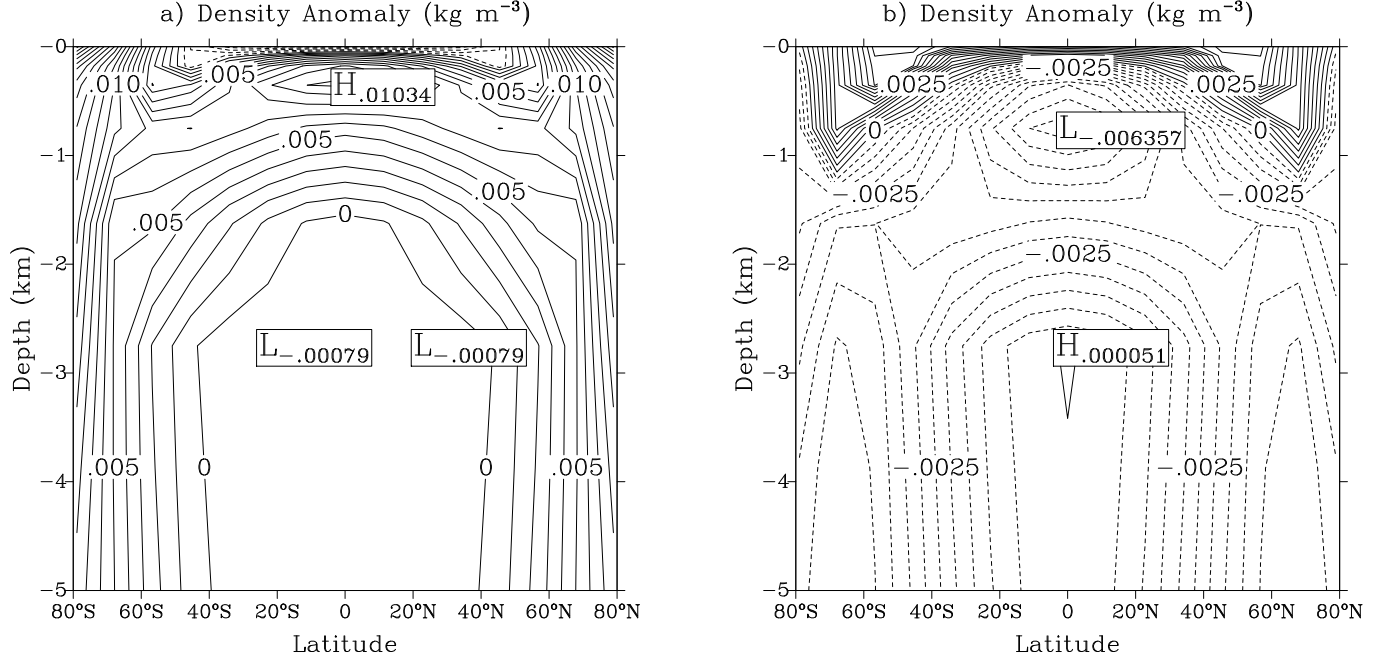


**Figure 3:** The real, (a), and imaginary, (b), parts of the density perturbation for the growing oscillatory eigenfunction for the two-cell circulation in the (2,1) case. In this case, and in all other oscillatory cases, the mode is symmetric in temperature, salinity and density and hence anti-symmetric in the streamfunction perturbation.

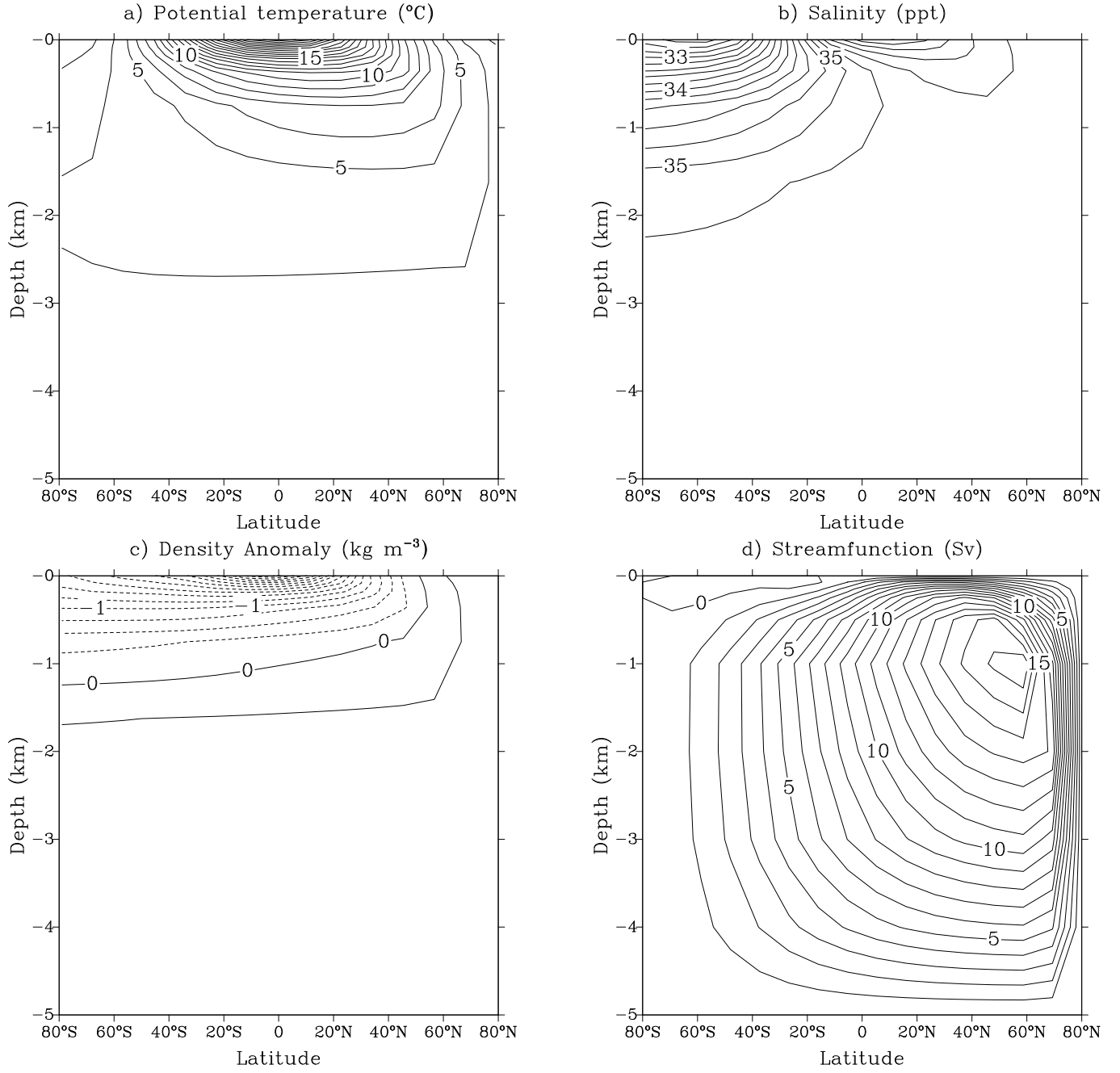


**Figure 4:** The (a) Temperature, (b) salinity, (c) density anomaly and (d) the streamfunction for the northern sinking one-cell circulation in the (2,1) canonical diffusivities case under mixed boundary conditions.

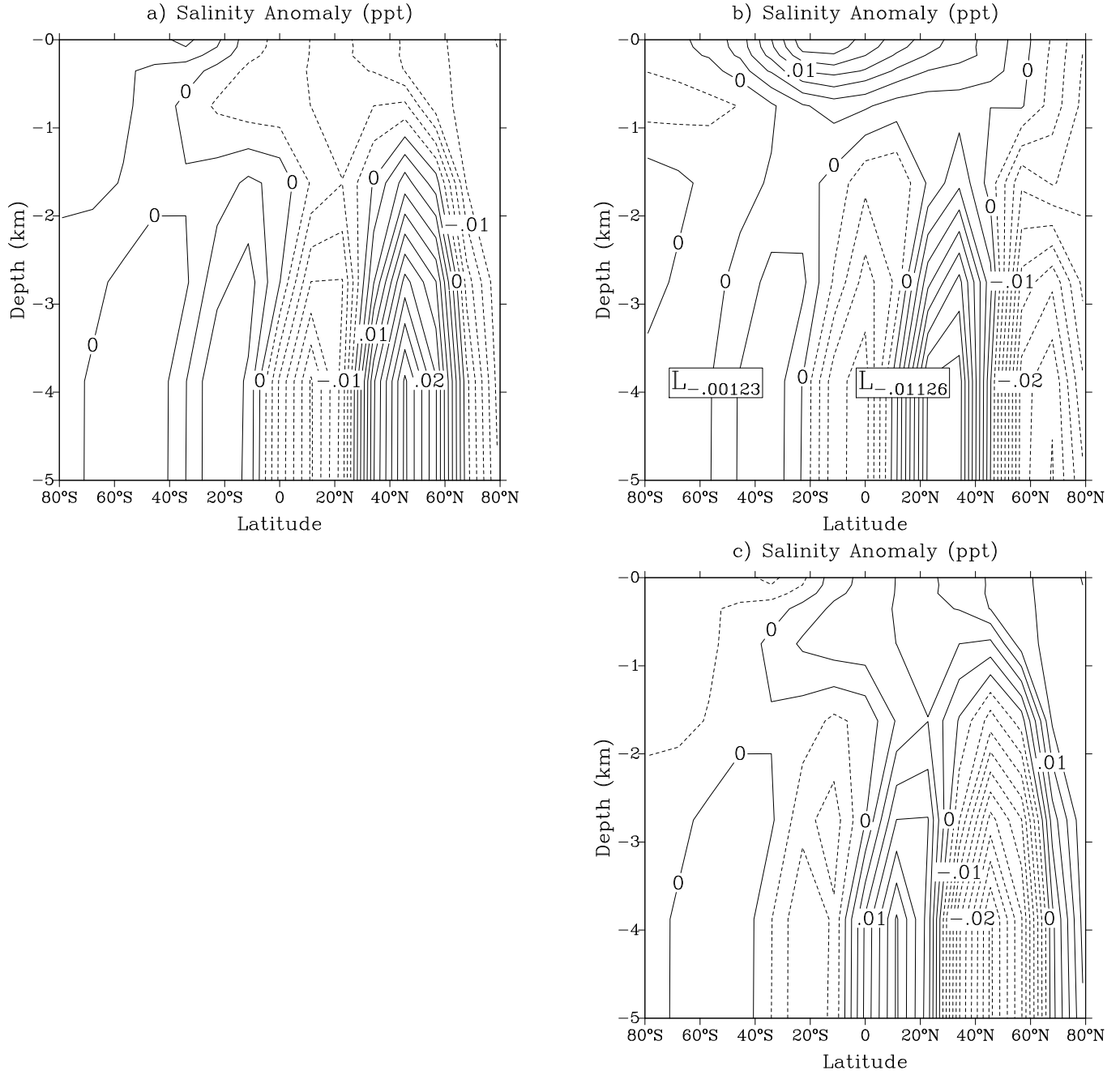


**Figure 5:** Snapshots at a)  $t = t_0$ , b)  $t = t_0 + \pi/2\omega$  and c)  $t = t_0 + \pi/\omega$ , of the salinity anomaly field over a half period ( $\approx 150$  yrs) of the sub-critical oscillation for the case (4,1). The following half period is simply this sequence multiplied by -1. It is clear that the salinity anomalies develop at the surface and are then advected clockwise by the main one-cell circulation.



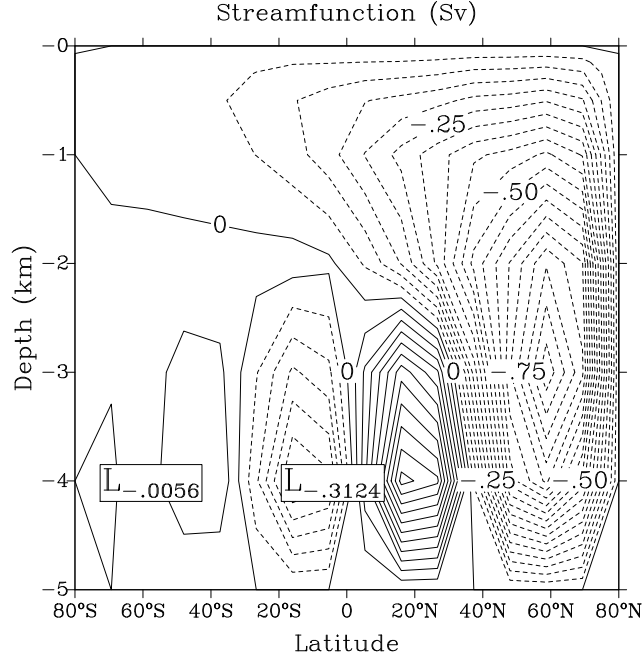


**Figure 6:** The anomaly in the streamfunction field for the case (4,1) due to the initial salinity perturbation show in Fig. 5a. Most of the perturbation is in the deep ocean where the basic state temperature and salinity fields are almost constant and hence has only a minor rôle in the propagation of the oscillation.

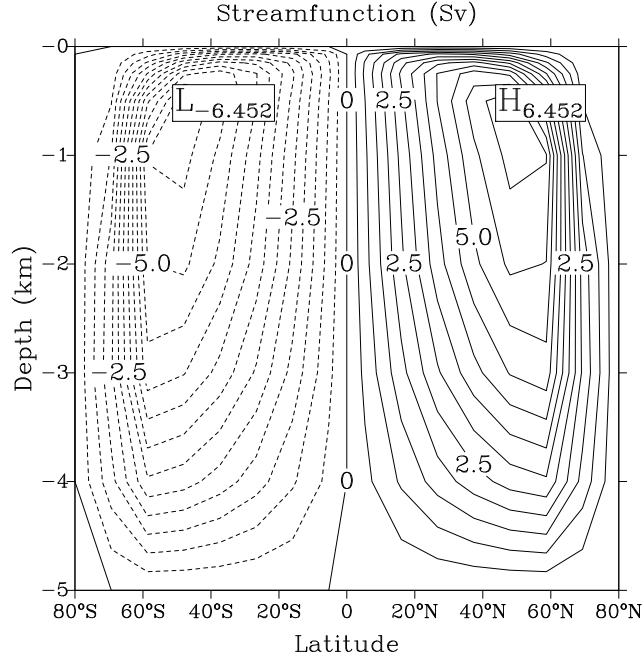


**Figure 7:** The streamfunction at steady state under restoring boundary conditions for the case where  $\tau_S = 600$  days and the  $\tau_T = 50$  days. The basic state has small pools of neutrally stable water at the poles and most convection and advection occurs in the neighbouring boxes. The anomalously fast growing perturbations to this basic state are concentrated solely in the surface polar grid boxes and are due to the large gradients in the convection scheme at the point of near-neutral stability.

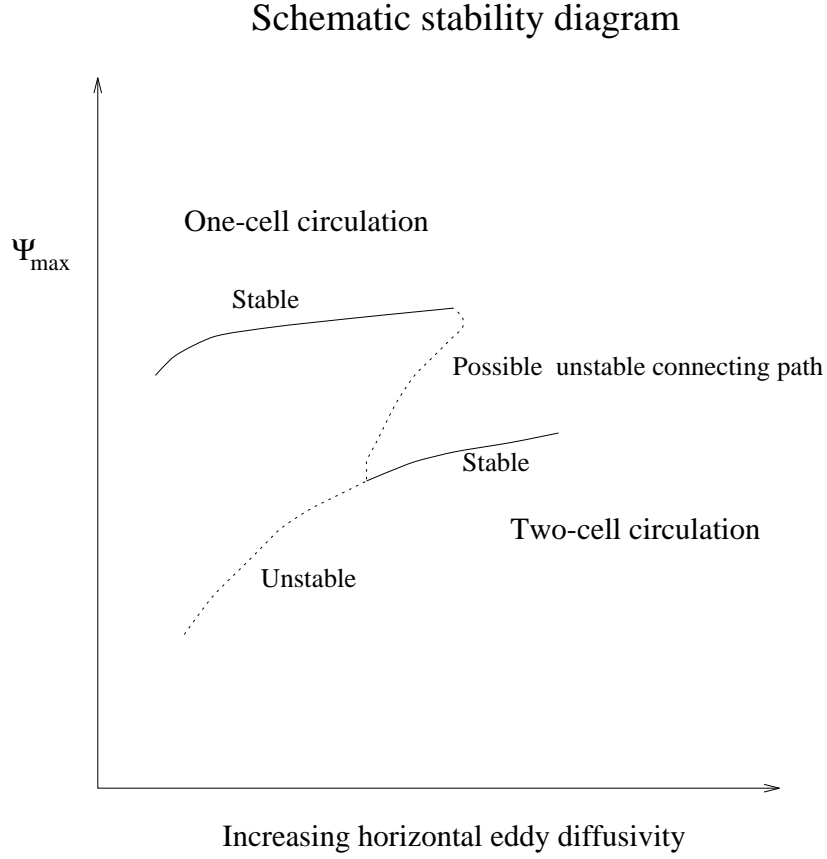


**Figure 8:** A schematic diagram showing the bifurcation structure of the model as the eddy diffusivities change. The horizontal diffusivity is increased while keeping the  $K_v$  and  $K_h$  at a constant ratio. The two steady states represented are the northern-sinking one-cell circulation (always stable if present) and the symmetric two-cell circulation. The two-cell pattern becomes stable as  $K_h$  increases and we conjecture that there is a pitchfork bifurcation at this point.